Macromolecules

ARTICLE

pubs.acs.org/Macromolecules

Time-Domain NMR Observation of Entangled Polymer Dynamics: Universal Behavior of Flexible Homopolymers and Applicability of the Tube Model

Fabián Vaca Chávez† and Kay Saalwächter*

Institut für Physik − NMR, Martin-Luther-Universität Halle-Wittenberg, Betty-Heimann-Str. 7, D-06120 Halle, Germany

ABSTRACT: Using a benchtop NMR spectrometer, we performed proton multiple-quantum NMR experiments to study the dynamics of well-entangled linear poly(butadiene), poly(isoprene), and poly(dimethylsiloxane) in a broad molecular weight range. The method provides a direct time-domain measurement of the segmental orientation autocorrelation function over many decades, based on time−temperature superposition. The function can be directly compared to theoretical predictions based on the tube model, and the Rouse and the disentanglement times can be evaluated relative to the known entanglement time. We obtain universal results for all three polymers when plotted against the molecular weight normalized by the entanglement molecular weight, with the familiar mass scaling exponents of 2.0 ± 0.2 and 3.2 ± 0.2, respectively. However, the time scaling exponent derived for motions in the constrained-Rouse regime II is not constant at the predicted value of −1/4 but is always larger and also a universal function of molecular weight. This observation was previously explained by constraint-release effects that are active at surprisingly short times and at local scales. We further discuss observations related to contour-length fluctuations, leading to an isotropically mobile fraction of segments that can also be quantified by our method.

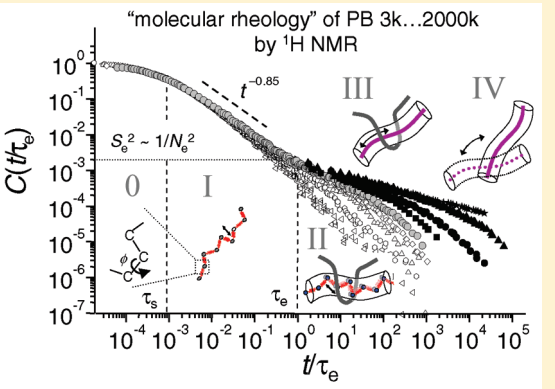

I. INTRODUCTION

Polymer liquids show dynamical properties that are of considerable scientific and technological interest. The dynamics of polymer melts with molecular weight $M_w \gg M_e$, with M_e as the molecular weight between two entanglements, is most successfully described by the tube model developed by Doi and Edwards[1] and is based on the famous concept of reptation originally proposed by de Gennes.[2] In essence, the complex topological interactions between neighboring chains are modeled by a fictitious tube around the chain referred to.

According to the tube model, the dynamics of a polymer chain far above the glass transition is complex and falls into different regimes depending on the length and time scales. At very short times, corresponding to the nanosecond and a few angstroms scales, the segments move freely, subject only to chain connectivity effects (regime I), which can be described by the Rouse model.[3] One should keep in mind that at even shorter times a truly molecular perspective must include subsegmental processes, the time scale of which is set by the α process ("glassy dynamics", regime 0), which essentially drives the segmental modes.[4] At longer times (nanoseconds−microseconds) and larger space scales, the polymer chain feels the constraints imposed by the surrounding chains ("tube"), and the corresponding regime II is referred to as constrained-Rouse, sometimes also "local reptation". Beyond this regime, the chain moves diffusively along the curvilinear tube, i.e., it reptates (regime III). Finally at very long times, free diffusion is established (regime IV). Figure 1 summarizes the dynamic regimes predicted by the tube/reptation model for the segmental mean-square displacement and the orientational autocorrelation function, which is the central observable for NMR methods probing anisotropic spin interactions. The power laws and the characteristic crossover times for the different dynamic regimes are also indicated.

The tube model further predicts a molecular weight scaling of the Rouse and the disentanglement times as $\tau_R \sim M_w^2$ and $\tau_d \sim M_w^3$, respectively, and these time scales are of direct rheological relevance. It is well established that, experimentally, the latter scaling exponent, as reflected in the M_w dependence of the viscosity, is found to be 3.3−3.5, and for an explanation, additional relaxation processes such as contour length fluctuations (CLF) and constraint release (CR) were suggested.[7−11] These processes alter the stability of the "tube" itself, and their respective relevance and details about their implementation in rheological models are still under active discussion.

The validity of the tube model can in principle be probed by adequately course-grained computer simulations. While the invention of primitive-path analysis (PPA) has provided a powerful tool to extract the microscopic parameters of a static tube constraint and thus predict correctly the plateau modulus of long-chain polymer melts from simulations,[12] current bead−spring models reach the terminal regime only for chains with about 10 entanglements.[13] PPA helps in deriving dynamic properties of

Received: November 11, 2010
Revised: January 25, 2011
Published: February 28, 2011

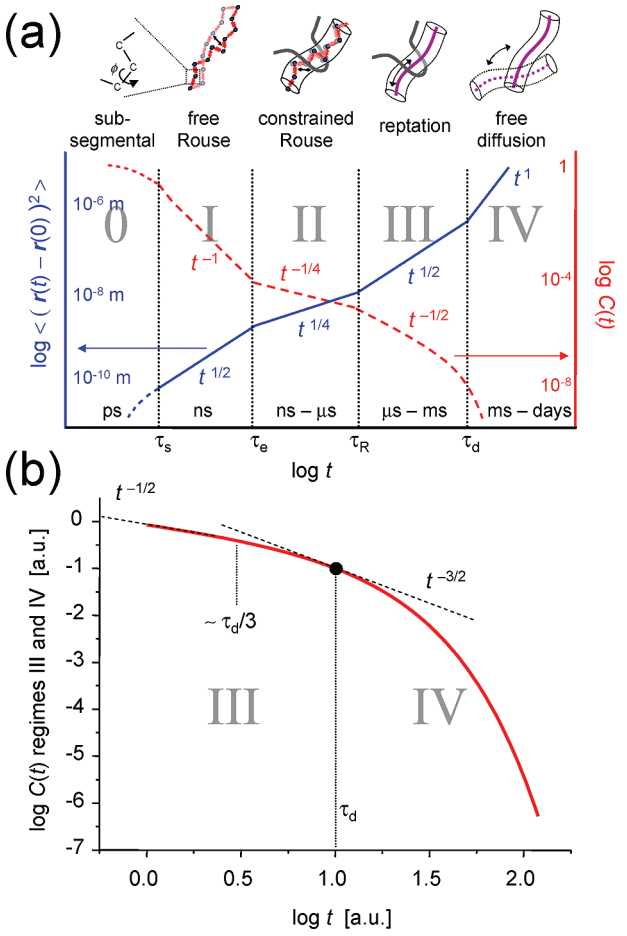

Figure 1. (a) Dynamic regimes and crossover times predicted by the tube/reptation model, observed for the mean-square displacement $\langle(\mathbf{r}(t) - \mathbf{r}(0))^2\rangle$ of segments (solid line, ref 1) and the rotation autocorrelation function $C(t)$ (dashed line, refs 2, 5, and 6). Regime transitions occur at the segmental (τ_s), entanglement (τ_e), Rouse (τ_R), and disentanglement (τ_d) times. (b) Close-up of $C(t)$ for regimes III and IV according to eq 1, where deviations from the $-1/2$ power law already start in regime III at around $\tau_d/3$.

the tube at shorter times[14] and is also used as a basis of mapping procedures to predict the rheological behavior for longer times.[15] In agreement with recent interpretations of rheological data,[10,16,17] the most recent simulation results[13,15,18] appear to stress an increasing importance of CR in particular at high molecular weights.

Innumerable experimental studies of polymer melts were carried out to test the predictions of the tube model, but molecular techniques, focusing in particular on the Doi–Edwards regimes II–IV (constrained Rouse, reptation, and terminal diffusion), stand out in that they are in principle able to test the fundamental model assumptions and can be compared directly to computer simulations. For instance, a direct visualization of reptation was possible for a single and flexible DNA polymer using fluorescence microscopy.[19] Further, dielectric,[20] neutron spin–echo (NSE),[21] and various NMR spectroscopy techniques[4,22−28] have been applied to study polymer dynamics at the atomic level.

The use of NMR, in particular of techniques relying on anisotropic spin interactions and thus rotational motions to study reptation, was in fact already pointed out by de Gennes in his seminal 1971 paper.[2] In short, most NMR experiments (with the exception of pulsed-gradient diffusion techniques) measure segmental dynamics ultimately in terms of an orientation autocorrelation function (OACF) of the second Legendre polynomial $C(t) = \langle P_2(\cos\theta(t))P_2(\cos\theta(0))\rangle$, where θ is the segmental orientation relative to a reference direction, i.e., the external magnetic field. As already shown by de Gennes, in regimes III and IV this OACF is proportional to the tube survival probability $\psi(t)$, which in turn is directly relevant for the calculation of rheological properties.[1,15] Thus, conventional proton and deuterium longitudinal and transverse relaxometry[6,28−33] as well as more advanced approaches such as solid-echo-based approaches,[34,35] the dipolar correlation effect,[36] and the β echo[5,37] have been used to study polymer melt dynamics. All these techniques have in common that they are directly sensitive to the anisotropy of segmental orientation fluctuations as imposed by the entanglements, leading to solidlike effects on the NMR signal due to residual anisotropic interactions, a concept that was pioneered by Cohen-Addad.[38]

In particular, the more recent work of Ball, Callaghan, and Samulski (BCS) has provided a consistent tube-model-based theoretical treatment of $C(t)$. In regimes III and IV, it is given by

$$C(t) \sim t^{-1/2}\psi(t) \sim t^{-1/2} \sum_{p\ \mathrm{odd}} \frac{8}{\pi^2 p^2} \mathrm{e}^{-p^2 t/\tau_d} \qquad (1)$$

which is plotted in Figure 1b.[5] We point out that the regime III–IV transition is smooth and not identified by a sudden change in the time-scaling exponent. The full $C(t)$ can be obtained from refs 28 and 39 or used to predict longitudinal and transverse relaxation phenomena as well as signal functions of more complex NMR experiments. As a direct and in some aspects improved alternative to the β echo of BCS,[5,37] multiple-quantum (MQ) NMR[26,39−41] has emerged as a powerful technique to investigate chain dynamics and local structure (cross-link and entanglement density) of polymer networks and melts.

In contrast to longitudinal relaxation methods, MQ NMR is based on fundamentally different principles, measuring a time integral of correlated dipolar couplings, thus $C(t)$, directly and model-free in the time domain[26,40] rather than deriving it from a spectral density, which has to be known for all frequencies in order to obtain $C(t)$ as its Fourier transform. The earliest magic-angle spinning (MAS) method of Graf et al.[26,40] is subject to systematic errors, and a simple static version, robust enough for a time-domain benchtop spectrometer, provides a smooth and artifact-free measure of $C(t)$. In a recent letter,[39] we have given a first account of the application to entangled 1,4-poly(butadiene), covering regimes II–IV of the tube model. We could determine the characteristic regime transition times, which exhibited the expected and familiar molar-mass scaling exponents. Importantly, we observed deviations from the tube-model predicions in the form of a mass-dependent time scaling exponent describing segmental fluctuations in the constrained-Rouse regime II up to very high molecular weights of around $1000M_e$, demonstrating that local chain motions are governed by modes that are much less restricted than predicted by the tube model. Besides that, results from experiments carried out on protonated chains diluted in deuterated (invisible) matrix chains suggested CR processes as the major origin.

In the present article, we extend our previous work and compare the dynamics of 1,4-poly(butadiene), PB, 1,4-*cis*-poly(isoprene), PI, and poly(dimethylsiloxane), PDMS, over a broad molecular weight range. We further provide more detailed background information on the analysis of the MQ NMR data, including the discussion of contributions from isotropically mobile

chain ends that are commonly associated with CLF effects. In the subsequent article,[42] we will present the use of the segmental OACF as a basis of a fully consistent analytical calculation of the time-domain NMR signal functions.

II. EXPERIMENTAL SECTION

Samples. Low-polydispersity 1,4-PI, 1,4-(*cis/trans*)-PB, and PDMS were purchased from Polymer Standards Service GmbH (PSS, Mainz, Germany), except PDMS 1000K, which was kindly provided by Thomas Wagner (MPI-P, Mainz, Germany). The sample names include the approximate M_w in Da; GPC characterization results were supplied by the provider. The samples were placed in 8 mm o.d. NMR tubes, flame-sealed under vacuum to avoid degradation, and were kept in the refrigerator at 4 °C before and after the measurements. The distribution of cis:trans:vinyl units in some of the PB samples was determined by ^{1}H magic-angle spinning NMR at 13 kHz rotation frequency in a Bruker Avance II 400 MHz spectrometer, and values of around 55%:40%:5%, respectively, commonly found for anionically synthesized samples, were confirmed (see Figure 2). For PI, the provider specifies a microstructure of cis:trans:3,4-vinyl of 66%:27%:7%.

NMR Experiments. Proton MQ NMR experiments were performed on a Bruker Minispec mq20 (B_0 = 0.47 T), with 90° pulses of about 3 μs length. The sample temperature was regulated and stabilized to within ±0.5 K by means of a Bruker BVT 3000 temperature control unit operating with gas flow, covering a temperature range between 230 and 400 K. The sample temperature was controlled via dry and cooled nitrogen gas below and via heated pressurized air above room temperature. The used MQ experiment is based on the pulse sequence published by Baum and Pines[44] and is described in detail elsewhere.[41] Basically, it excites all even quantum orders, and using appropriate phase cycling, the pulse sequence yields a buildup curve dominated by double-quantum (DQ) coherences (I_{DQ}) and reference decay curve (I_{ref}) as a function of pulse sequence time τ_{DQ}, which is incremented in small steps by adjusting the interpulse spacings of basic two-cycle excitation and reconversion intervals. The full magnetization, subject only to incoherent relaxation processes and thus used to normalize the signals, is then obtained as $I_{\Sigma MQ} = I_{DQ} + I_{ref}$.

In terms of phase evolution, with the dipolar phase

$$\phi(t_a, t_b) = D_{eff} \int_{t_a}^{t_b} P_2(\cos \beta_t)\, dt; \quad t_b - t_a = \tau_{DQ} \tag{2}$$

the signal functions for an effective spin pair can be written as

$$I_{DQ} = \langle \sin \phi_1 \sin \phi_2 \rangle \tag{3}$$

$$I_{ref} = \langle \cos \phi_1 \cos \phi_2 \rangle \tag{4}$$

$$I_{\Sigma MQ} = \langle \sin \phi_1 \sin \phi_2 \rangle + \langle \cos \phi_1 \cos \phi_2 \rangle \tag{5}$$

where $\phi_1 \equiv \phi(0, \tau_{DQ})$ and $\phi_2 \equiv \phi(\tau_{DQ}, 2\tau_{DQ})$. The brackets here denote an ensemble (spatial) average, and we note that the dynamic information is encoded in the statistically fluctuating orientation of the internuclear vector, β_t. Note that the real system is characterized by a multitude of interacting nuclear dipoles, and thus the dipole−dipole coupling constant $D_{eff}(M_{2eff})^{1/2}$ is an effective one, representing a second-moment-type quantity $\sim[\sum D_{ij}^2]^{1/2}$.

Note further that the double-quantum signal function, I_{DQ}, given by eq 3, is completely analogous to the sin−sin correlation function first treated explicitly by the Mainz group,[35] who obtained it by manual combination of separate FID and solid-echo data sets. The β echo as introduced by BCS[5,37,45] represents an improved version that can be measured in a single experiment; it is also a purely dipolar buildup function, internally compensated for dephasing due to Zeeman precession. There is only one important difference: the long-time behavior of the β echo (and its predecessors) suffers from the fact that the experiment consists of two free (dipolar) evolution intervals, where second-order effects related to the noncommutativity of dipole−dipole couplings involving different spins become relevant, equivalent to the failure of a solid echo in reversing dipolar time evolution. This problem is not present for the used MQ pulse sequence, which features a clean DQ Hamiltonian, providing perfect time reversal upon applying the correct phase cycling, leading to cleaner signal functions.[41] While BCS focused their in-depth analysis only on this function, we will highlight below and in the subsequent paper[42] that including the cos−cos function is beneficial in that more specific information can be derived from a combined analysis.

For a theoretical treatment, we follow BCS[5] and our previous work on MQ experiments on elastomers,[46] assuming that the interaction

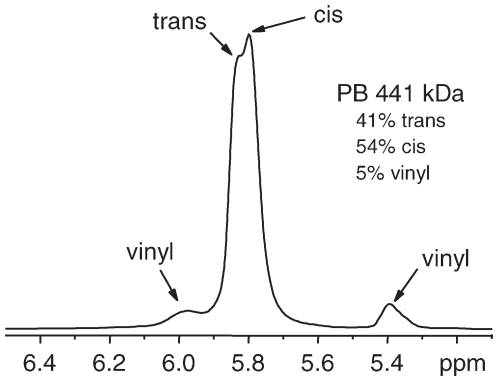

Figure 2. ^{1}H MAS NMR spectrum (13 kHz spinning frequency) of PB 441K. Integration/deconvolution yields a content of cis:trans:vinyl units of 54%:41%:5%, respectively.

Table 1. Characteristics and NMR-Determined Dynamic Parameters of the Investigated PB, PI, and PDMS Samples[a]

sample	$\overline{M}_w$	PD	Z	$\log(\tau_R/\tau_e)$	$\log(\tau_d/\tau_e)$	ϵ
PB 23K	23.6	1.01	12	1.3 ± 0.1	3.24 ± 0.02	0.44 ± 0.02
PB 35K	35.0	1.01	18	1.9 ± 0.1	4.10 ± 0.02	0.43 ± 0.02
PB 55K	55.3	1.02	29	2.2 ± 0.1	4.78 ± 0.07	0.39 ± 0.03
PB 87K	87.0	1.01	45	2.9 ± 0.1	5.10 ± 0.04	0.36 ± 0.01
PB 196K	196	1.02	102	3.3 ± 0.1	6.6 ± 0.2	0.31 ± 0.01
PB 441K	441	1.07	228			0.31 ± 0.01
PB 2000K	2000	1.02	1036			0.29 ± 0.01
PI 17K	17.6	1.02	2.8		1.61 ± 0.03	
PI 21K	21.2	1.03	3.3		2.03 ± 0.03	0.56 ± 0.02
PI 47K	47.3	1.01	7.4		3.11 ± 0.04	0.48 ± 0.02
PI 85K	85.4	1.01	13	1.64 ± 0.03	3.53 ± 0.08	0.44 ± 0.01
PI 110K	110	1.01	17	1.97 ± 0.05	3.81 ± 0.06	0.41 ± 0.02
PI 157K	157	1.01	25	2.29 ± 0.03	4.6 ± 0.1	0.36 ± 0.02
PI 360K	364	1.03	57			0.34 ± 0.01
PI 760K	735	1.04	115			0.31 ± 0.01
PI 1000K	999	1.05	157			0.31 ± 0.01
PDMS 128K	128	1.13	11		3.47 ± 0.04	0.50 ± 0.02
PDMS 166K	166	1.06	14	1.9 ± 0.03	3.67 ± 0.04	0.41 ± 0.02
PDMS 1000K	1000	1.70	83			0.36 ± 0.01

[a] Weigth-average molecular weight ($\overline{M}_w$) in kDa, polydispersity (PD = $\overline{M}_w/\overline{M}_n$), number of entangled chain segments $Z = \overline{M}_w/M_e$, characteristic times of the tube model τ_R and τ_d in multiples of τ_e, and the regime II time-scaling exponent ϵ. The M_e of PB, PI, and PDMS taken from ref 43 are 1.93, 6.37, and 12 kDa, respectively.

dx.doi.org/10.1021/ma1025708 |*Macromolecules* 2011, 44, 1549–1559

frequency distribution is Gaussian, which means that the Anderson−Weiss approximation[47] can be used to solve the nontrivial problem of proper ensemble averaging. In a first step, one obtains

$$I_{DQ} = \sinh\langle\phi_1\phi_2\rangle e^{-\langle\phi_1^2\rangle}$$

$$I_{ref} = \cosh\langle\phi_1\phi_2\rangle e^{-\langle\phi_1^2\rangle}$$

$$I_{\Sigma MQ} = e^{\langle\phi_1\phi_2\rangle} e^{-\langle\phi_1^2\rangle}$$

where the ensemble average is now to be taken over the individual phases, which is a rather straightforward exercise.[48] Details on the full analytical treatment and a critical discussion are deferred to our subsequent paper;[42] we here merely note that the averages in the above equations reduce to simple integrals over the OACF $C(|t_b - t_a|) = \langle P_2(\cos\beta_{tb})P_2(\cos\beta_{ta})\rangle$.

III. RESULTS AND DISCUSSION

MQ Raw Data Treatment and Interpretation. We have measured the I_{DQ} and I_{ref} signals over a broad range of molecular weights above M_c and in a temperature range above T_g from 240 to 400 K for three linear polymer melts: PB, PI, and PDMS. In Figure 3a we present a typical M_w dependence of DQ buildup raw data, just intensity-normalized with respect to 1.0 representing the full magnitization after a 90° pulse. In the lower M_w range, we observe a strong increase in the initial slope and an increasing maximum intensity. This directly reflects the effect of the entanglements on the magnitude and time stability of the apparent residual dipolar coupling D_{res}, which in turn is given by $[C(\tau_{DQ} \simeq 1\ \text{ms})]^{1/2}$. From this, one can qualitatively conclude that $C(t)$ is increasingly flat at around the time scale set by the DQ buildup, meaning that we move from regime IV to regime II dynamics in the given M_w range at the given time scale of 1 ms at 303 K. The temperature dependence of I_{DQ} and I_{ref} for the given sample PB 87K is shown in Figure 3b. The strong variation with T is again due to a transition from regime IV to regime II dynamics upon cooling.

The composite signal function $I_{\Sigma MQ}$ represents the fully dipolar-refocused magnetization, and it is here employed to obtain the normalized DQ intensity, I_{nDQ}, to be used in further analysis. As established in our previous work,[46] the decay of $I_{\Sigma MQ}$ is primarily influenced by segmental motions that are faster than the τ_{DQ} time scale, while I_{DQ} is governed by the strong additional sensitivity to intermediate and slow motions. The fast-motion contribution can thus be factored out via a point-by-point division through $I_{\Sigma MQ}$, provided that both quantities contain signal from the same molecular species.

However, one has to keep in mind that the latter contains signal from isotropically mobile segments (chain ends, etc.), which do not lead to measurable DQ intensity. This fraction is most reliably identified by plotting $\log(I_{ref} - I_{DQ}) = \log I_{\Delta MQ}$ vs τ_{DQ}.[49] It is based on the notion that, neglecting chain ends, $I_{\Delta MQ} = \langle\cos(\phi_1 + \phi_2)\rangle$, as seen from eqs 3 and 4. This is equivalent to a Hahn echo,[46] i.e., dephasing of the dipolar coupled part, which of course emphasizes the slower relaxation of the "isotropic tails". These can then be quantified by a single-exponential fit to the long-time data (see Figure 4). Ultimately, the correct normalized DQ (nDQ) intensity is obtained as

$$I_{nDQ} = \frac{I_{DQ}}{I_{ref} + I_{DQ} - f\exp(-2\tau_{DQ}/T_2^{tail})} \qquad (6)$$

The inset in Figure 3b presents the corresponding nDQ intensities for the same data set. The observed strong variation of I_{nDQ} is a clear signature of reptation dynamics, while it is nearly T-independent in the case of cross-linked polymers,[46] indicating

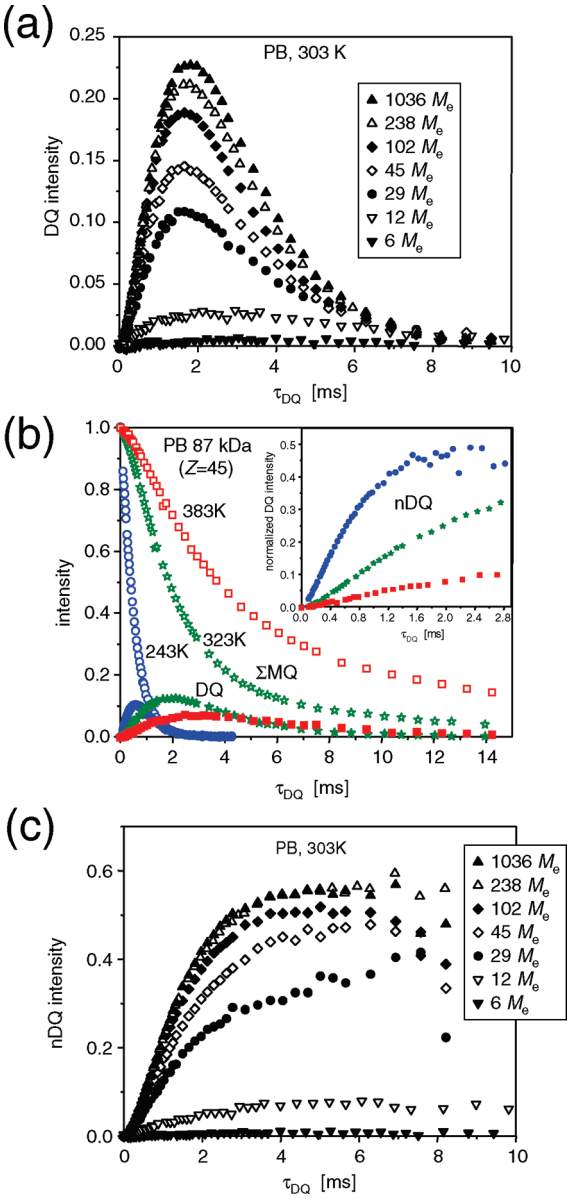

Figure 3. (a) Molecular weight dependence of I_{DQ} for PB ranging from 6 to 1100 M_e. (b) Typical temperature dependence of I_{ref} and I_{DQ} observed in polymer melts, here for the example of PB 87K. The inset shows the normalized DQ signals (see text). (c) Relaxation-corrected (normalized) I_{nDQ} data corresponding to (a). The effects of entanglements and large-scale motion are directly reflected in the initial slope and the intensity of the signals.

the complete absence of long-time relaxation in permanent networks, where $C(t)$ has a long-time plateau. This is stressed by the data presented in Figure 3c, which is the nDQ data corresponding to the raw data in Figure 3a. The long-time signal relaxation due to segmental dynamics is removed, leaving slow-motion effects, i.e., increasingly isotropic motion due to faster reptation of short chains as the origin of the low signal for low M_w. At high M_w, the nDQ buildup is network-like, revealing strongly anisotropic chain motion as a result of the entanglement constraints.

Chain-End Dynamics and CLF. Before we turn to a closer analysis of I_{nDQ}, we explore the isotropic end fraction in some more detail. Doi identified the chain-end dynamics, now referred

dx.doi.org/10.1021/ma1025708 |Macromolecules 2011, 44, 1549–1559

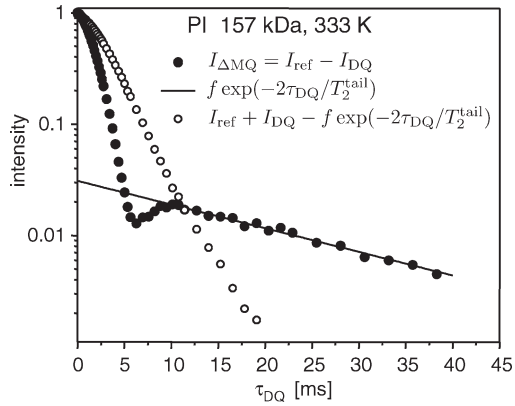

Figure 4. Procedure to extract the slowly relaxing part associated with isotropically mobile chain segments in the MQ signals. See text for details.

to as CLF in the framework of tube models, as a possible reason for the large (>3) exponent in the mass scaling of the terminal time and the viscosity.[50] While the final conclusion is still a matter of current debate, the interpretation of the chain-end influence on the stress relaxation modulus is rather descriptive, in that it serves as "diluent" of the entangled fraction, with $G \sim G_0[1 - \mu(M/M_e)^{1/2}]$.[50] The second part in the sum represents the isotropic fraction that bears no load, and the fraction is thus predicted to scale with $M_w^{-1/2}$.

Isotropic fractions have previously been identified in ^{1}H and ^{2}H NMR T_2 and line-shape studies of polymer melts as well as elastomers,[51] and the most complete study for polymer melts is due to Kimmich et al.,[52] who found an approximate M_w^{-1} behavior for poly(ethylene), PDMS, and poly(tetrahydrofuran). We note that the fits in this work are only based on 3−4 data points each, and closer inspection reveals that a lower exponent could still be reconciled with the data in the higher M_w range. A possible interpretation of the M_w^{-1} is that $2M_e/M_w$ trivially represents the unentangled end fraction in any linear chain, while a proper theory of course has to take into account the observed increase at increasing temperature. This is on the one hand due to reptation itself[50] but, as pointed out by Kimmich, could also be due to the formation of hairpin-like loops that "stick out" of the tube in the center part of a chain. In a thorough study of Cohen-Addad using end-deuterated pseudo-triblock copolymers of PB, it was indeed shown that a significant fraction of the isotropic part must be associated with the chain center,[53] stressing the nontrivial origin of this fraction.

Figure 5 presents values of the chain-end fraction f for some PB and PI samples obtained from our MQ experiments as a function of temperature. The insets further show the molecular weight dependence for all studied PB and PI samples at 303 and 313 K, respectively. The fractions decrease as either the temperature or M_w increases, and from the insets we take mass scaling exponents on the order of 0.65 ± 0.1, which is not much larger than Doi's predicition, yet smaller than (but still compatible with) the data of Kimmich et al. We stress that significant fractions ≫10% are only obtained for the lowest-M_w samples and at the highest temperatures, and in this range, the tail fraction is not as well separated as in Figure 4, leading to ambiguities. We stress, however, that the rather small end fraction and possible uncertainties in its determination of the order of a few percent do not challenge any of the results drawn below from I_{nDQ} calculated by eq 6.

Analysis of nDQ Buildup Data. For the case of polymer melts it was shown by Graf et al.[26,40] that for short τ_{DQ} the nDQ

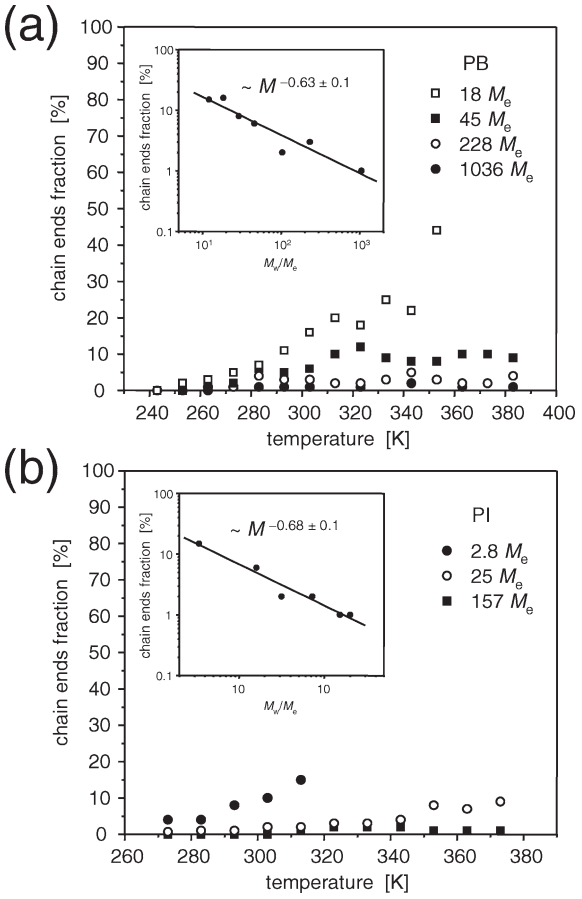

Figure 5. Chain-end fractions of some (a) PB and (b) PI samples as a function of temperature. The insets show a log−log plot of the M_w dependence for all PB and PI samples studied at 303 and 313 K, respectively, with solid lines as fits to determine the scaling exponents.

intensity is proportional to the OACF on the time scale of τ_{DQ}, $I_{nDQ}(\tau_{DQ}) \propto C(\tau_{DQ}) \times \tau_{DQ}^2$. This provides a means for a direct time-domain measurement of $C(t)$, and the advantage of our robust static MQ experiment vs the MAS version of Graf et al. is that the time axis is not limited to a few points dictated by one or even multiple rotor periods but can be probed continuously, starting at a minimum τ_{DQ} of around 100 μs (depending on the pulse lengths). Note that the approximation works best when the faster (regime 0, I) processes, that constitute the major relaxation channel of $I_{\Sigma MQ}$, are normalized away via the nDQ calculation, constituting a significant advantage over the β echo. This will backed up with theoretical calculations in our subsequent paper.[42]

We first focus on the possibility to obtain the power law exponent of $C(t)$ in a short time range from a single MQ experiment in a completely model-free way. In Figure 6a,b we plot the logarithmic nDQ buildup vs log τ_{DQ} and perform a linear fit to the initial data points up to a value of around $I_{nDQ} \approx 0.05$. Note that such fits need to be performed in logarithmic units, and they have to be weighted according to the error intervals, which are estimated from the (constant) experimental noise, but vary on a log-scale, so as to not overestimate the initial points that suffer from low signal. Since $C(\tau_{DQ}) \propto I_{nDQ}(\tau_{DQ}) \times \tau_{DQ}^{-2} \sim \tau_{DQ}^{-\varepsilon}$, the so-obtained slopes correspond to $2 - \varepsilon$.

Results for the resulting power-law exponent of $C(t)$ for PB 87K are plotted in Figure 6c as a function of temperature, and they are compared to the result of the unexpectedly high ε value

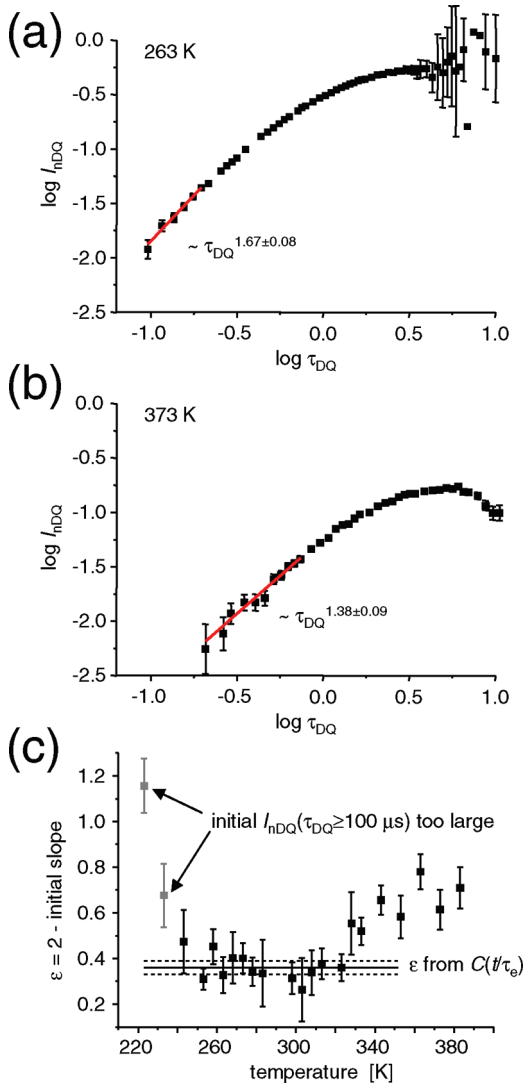

Figure 6. (a, b) Log−log plot of $I_{nDQ}(\tau_{DQ})$ vs τ_{DQ} for two different temperatures (sample PB 87K), with linear fits to the initial parts. (c) Power law exponent ε calculated from the initial slopes as a function of temperature. The corresponding regime II result with its confidence interval as obtained from the analysis of the full $C(t)$ on the basis of time−temperature superposition (see Figures 7 and 8) is also indicated.

obtained from the analysis based on time−temperature superposition (see below and ref 39). The simple slope analysis thus confirms the central result of our earlier work, namely, that the time scaling exponent in regime II always exceeds the tube model prediction of 1/4. We finally note that a reliable initial-slope analysis is possible due to the virtual absence of any pulse-sequence imperfections, which could challenge DQ excitation efficiency, thus delaying the initial DQ intensity buildup. This would lead to potentially overestimated values for ε.

Determination of the Complete OACF. Since the temperature range of our study is limited to probing the dynamics in regimes II−IV, and since the influence of faster (regime 0, I) processes is essentially taken care of by the normalization procedure, we follow refs 26 and 40 and factorize the OACF according to $C(t > \tau_e) = C(\tau_e) \times C_e(t > \tau_e)$ with $C_e(t \leq \tau_e) = 1$ and use

$$I_{nDQ}(\tau_{DQ} > \tau_e) = AS_e^2\tau_{DQ}^2C_e(\tau_{DQ}) \quad (7)$$

Table 2. Experimental and Literature Parameters for the Three Investigated Polymers[a]

	PB	PI	PDMS
$D_{res}/2\pi$ [Hz]	100 ± 30	110 ± 15	90 ± 10
S_e	0.045	0.021	0.024
$N_{e,exp}$	13	21	25
$N_{e,lit}$	18	30	32
b [Å]	9.6	9.3	13
T_g [K]	174	206	150
T_{VF} [K]	126	161	100
ξ_0 [N s m^{-1}]	1.0×10^{-14}	4.0×10^{-14}	2.4×10^{-13}
α [K^{-1}]	7.10×10^{-4}	7.17×10^{-4}	1.44×10^{-3}
references	43, 55	43, 55	43, 56

[a] The values for D_{res}, the corresponding order parameter $S_e = (C(\tau_e))^{1/2}$, and number of Kuhn segments between two entanglements, $N_{e,exp}$, were determined herein, while references are given for the literature parameters used in eq 9 to calculate the entanglement time τ_e.

to obtain a small section of $C_e(\tau_{DQ})$ directly from the nDQ data, simply by dividing through τ_{DQ}^2. $S_e = (C(\tau_e))^{1/2}3/(5N_e)$ is the entanglement-induced local dynamic order parameter, which depends on the number of Kuhn segments between two entanglements, N_e, and A is a numerical factor. For a complete determination of $C(t)$, both its absolute value need to be fixed, and several orders of magnitude in time have to be covered.

The absolute value of $C(\tau_{DQ}) = S_e^2C_e(\tau_{DQ}) = (D_{res}k/D_{stat})^2$ (yielding A in eq 7) can be calculated as the ratio of the apparent D_{res} and a quasi-static reference value D_{stat}/k. The latter depends on the spin dynamics and the motions within a nominal Kuhn segment and was determined approximately for the three polymers studied here:[54] $2\pi \times 8.1$ kHz (PB), $2\pi \times 6.3$ kHz (PI), and $2\pi \times 7.6$ kHz (PDMS). An estimate of D_{res} at a certain temperature can be extracted from I_{nDQ} using a generic second-moment-based buildup function

$$I_{nDQ} = \frac{1}{2}\left[1 - \exp\left(-\frac{2}{5}D_{res}^2\tau_{DQ}^2\right)\right]\exp(-2\tau_{DQ}/T_2^{app}) \quad (8)$$

which includes an apparent damping term. Note that for PB, which is roughly a 50/50 mixture of cis and trans units, we use a two-component function, as explained in ref 39. Such superposed buildup functions (with potential D_{res} distributions) but without the T_2 term are normally used for permanent networks, for which I_{nDQ} is temperature-independent and reaches a long-time plateau of 0.5.[41] For melts, the fit yields good values for the highest M_w and temperatures at which the nDQ intensities close to 0.5 are reached (i.e., in regime II, where $C(t)$ has a weak decay).

We followed this procedure for each polymer (see ref 39 for details on PB), and the results for D_{res} are given in Table 2. Thus, the absolute value of $C(\tau_{DQ} \simeq 1\ ms)$ is obtained as 3×10^{-4} (PI at 343 K), 1.4×10^{-4} (PDMS at 243 K), and 1.5×10^{-4} (PB at 303 K), fixing the factor A in eq 7 for each polymer. Conservatively, noting the model dependencies of the D_{stat}/k values (which in fact is the only model dependence), the error in the absolute values of $C(t)$ is estimated to be on the order of 40%. This treatment corrects another problem of refs 26 and 40, where the used MQ pulse sequence suffered substantial intensity loss due to experimental imperfections, which means that no absolute-value fit for a determination of D_{res} was possible. The authors had

to resort to a calibration based on MAS sideband intensities, which apparently gave incorrect values. Along with later disproven assumptions[54] on specific intrasegmental proton pair coupling directions, the authors obtained a grossly overestimated local order, spawning a number of controversial discussions.

Following ref 39, we construct $C(t/\tau_e) \propto I_{nDQ}/\tau_{DQ}{}^2$ on the basis of the well-known and widely used time−temperature superposition (TTS) principle. Via a combination of data for a large set of temperatures, the envelope $C(t)$ is easily obtained by referencing the time axis to the known τ_e calculated according to

$$\tau_e \simeq \frac{\xi(T)b^2N_e{}^2}{\kappa k_B T} = \tau_s(T)N_e{}^2 \qquad (9)$$

where $\xi(T) = \xi_0 \exp\{[\alpha(T - T_{VF})]^{-1}\}$ is the monomeric friction coefficient, b is the Kuhn segment length, and T_{VF} is the Vogel−Fulcher temperature which is around 50 K lower than T_g. The literature[1,57] does not provide a consistent value for the numerical factor κ in the denominator, where the given values range between unity and $6\pi^2$. For our evaluations, we followed refs 26 and 40 and used $\kappa = \pi$. The other parameters used to calculate τ_e are found in the literature and are also listed in Table 2. In this way, a given τ_{DQ} is easily equated to t/τ_e by division trough $\tau_e(T)$. Restricting the MQ data to the initial time range, the full $C(t)$ is finally obtained; see Figure 7a for data for PB 2000K ($Z = 1036$) as an example.

These data, for chains with >1000 entanglements, in fact constitute the most important set, since we observe that the log−log slope of the composite $C(t)$ is constant over 4 orders of magnitude in effective time, evidencing an extended regime II with a well-defined time-scaling exponent. In fact, $\varepsilon = 0.29$ is the lowest value observed in our work.

With the full correlation functions given on a properly referenced time scale, it is now possible to extract the value at $C(\tau_e)$, which is extrapolated to about 2×10^{-3} (PB), 8.8×10^{-4} (PI), and 6.6×10^{-4} (PDMS). This immediately yields the parameters S_e and N_e, which are listed in Table 2. We see that the latter results, which reflect the tube diameter $d_T \simeq N_e{}^{1/2}b$, are 20−30% smaller than the literature values, yet reassuringly, the order of the 3 polymers is conserved. This indicates a systematic error for our reference values D_{stat}/k, which are probably too low. Presumably, our simplistic model based on spin dynamics in an isolated chain segment does not take proper account of interchain dipolar couplings.[54] We have indeed observed that isotopic dilution lowers the experimental apparent D_{res} by about 25%,[39] confirming the hypothesis. Further, our model was based on an extended arrangement of monomers inside the Kuhn segment, with rotational motions as a crude representation of the subsegmental dynamics. More insights should arise from incorporating atomistic molecular dynamics simulations,[58] taking full account of the local conformational dynamics.

With $C(\tau_e)$ now fixed, we obtain an absolute-value $C(t)$ for each sample, and we can compare our data with complementary data from T_1 field-cycling NMR published by Rössler and coworkers,[28] as already discussed in ref 39 (see Figure 7b). The agreement is near perfect and demonstrates the complementarity of the two techniques, which are both based upon TTS, yet rely on rather different principles, namely a direct time-domain measurement in our case and full frequency-space coverage and subsequent Fourier transformation in the latter case, based on the applicability of Redfield relaxation theory. This theoretical approach is very different from the short-time second-moment approximation used herein and states that $1/T_1$ is proportional to the spectral density $J(\omega)$, which is the Fourier transform of $C(t)$.

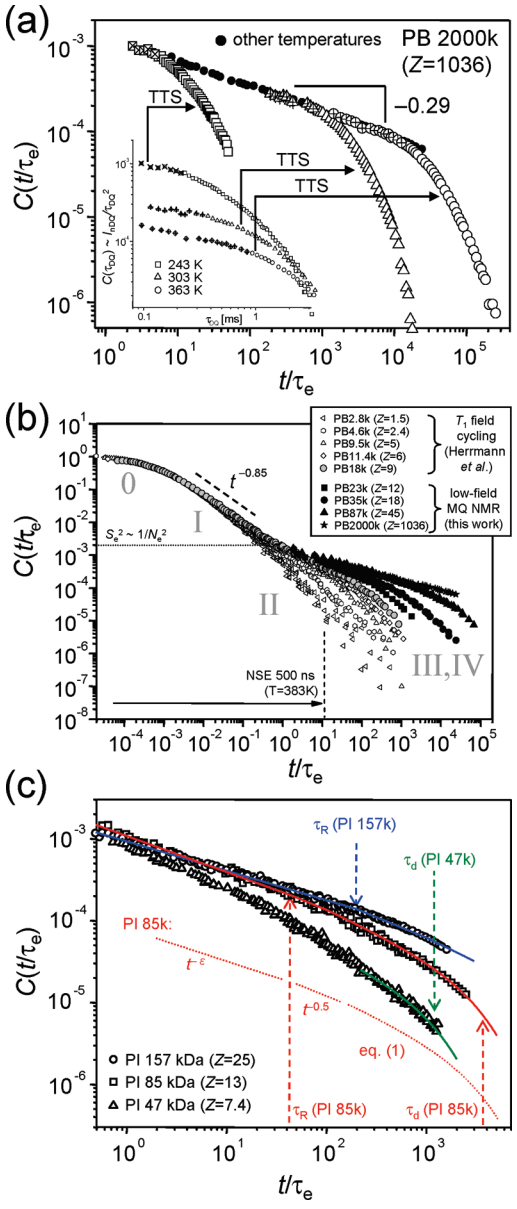

Figure 7. (a) Master curve for $C(t/\tau_e)$ obtained by TTS on the example of PB 2000K. Crossed symbols denote the part of the buildup curves that conforms to the initial-rise approximation ($I_{nDQ} < 0.05$). The inset shows $I_{nDQ}/\tau_{DQ}{}^2 \propto C(\tau_{DQ})$ traces subject to TTS; note that no vertical shift is applied. (b) $C(t/\tau_e)$ for PB, combined with field-cycling NMR data from ref 28 covering the lower time range, with no relative shifts applied. The dashed line indicates the approximate time limit for complementary NSE spectroscopy at the highest studied temperature. (c) Selected correlation functions for different PI samples. The lines correspond to the fits used to extract τ_R, τ_d, and the scaling exponent ε, with the fits to PI 85K being offset for clarity.

A chain length of $Z \approx 10$ marks the current upper applicability limit of field-cycling relaxometry for $C(t)$ determination, as the full frequency space down to the lowest frequencies reaching the Debye limit needs to be covered in order to reliably extrapolate the $1/T_1$ to infinitely small Larmor frequencies. The accessibility of lower frequencies is challenged by the difficult compensation of the Earth's magnetic field, at which $\omega_L/2\pi \approx 2$ kHz, and further, the applicability of standard relaxation theories at such low frequencies remains to be scrutinized.

dx.doi.org/10.1021/ma1025708 |Macromolecules 2011, 44, 1549–1559

We emphasize that we have an absolute-value comparison along both axes, with only a trivial change of the time reference. Using $\kappa = \pi$ in eq 9, the data sets and the extracted regime transition times match well when $\tau_s \simeq 4\tau_\alpha$.[64] The factor of 4 merely arises from a comparison of respective literature data[55,59] and makes sense from a phenomenological point of view, as several conformational jumps (α process) are needed to effectively relocate and thus relax a Kuhn segment, which is the meaning of τ_s. This issue is routed deeply at the connection between molecular reality (with τ_α being accessible by suitable NMR methods or dielectric spectroscopy) and coarse-grained chain models (for which τ_s results from extrapolations of model fits to, e.g. rheological or simulation data) and clearly deserves further investigations.

Dynamic Regimes and Tube-Model Parameters. Once the correlation functions were constructed for all samples, the next step was to extract characteristic regime transition times based on the predictions for $C(t)$ for the tube model (Figure 1), and noting the obvious deviation already discussed, the scaling exponent ε for regime II. See Figure 7c for sample data. Note that all fits need to be performed in log−log units. The parameter ε is determined first by exploring the slope in the early time region above τ_e, which now yields rather well-defined values with a smaller error interval as compared to the single-set analysis presented in Figure 6a,b. With ε fixed, τ_R is easily located by fitting two straight lines with fixed slope, taking $-1/2$ as the expected regime III slope,[5] fitting parameters being the prefactor (y value) and the crossover time. Finally, τ_d is determined by fitting (the logarithm of) eq 1 to data beyond τ_R. It should be mentioned that regimes III and IV were not reached for all samples studied here, in particular at high M_w. This was due to technical limitations because it implies to measure at high temperatures with the risk of sample decomposition.

The results for τ_R and τ_d are shown in Figure 8a for all samples, including field-cycling data of Rössler and co-workers for the lower M_w range which we have reanalyzed following the above fitting procedures. Within our experimental errors, which are mainly determined by the use of cheap low-field NMR equipment, and could further be due to systematic errors in the GPC-based M_w determinations, the molecular-weight dependence of τ_R agrees with the tube model prediction ($\sim M_w^2$). For τ_d, the exponent is higher than the predicted value of 3, but this is of course expected, as this is also observed for the melt viscosity or the terminal relaxation time from rheological experiments. Only above an even higher $M_{rept} \simeq 200M_e$, recent work indicates that the expected scaling is observed.[60]

On the whole, Figure 8 is a convincing demonstration that for flexible homopolymers, we observe universal behavior independent of the specific type of polymer, backing the validity of our experimental approach. From Figure 8b, we take that the clear molecular weight dependence of the exponent in the constrained-Rouse regime is also a universal feature of entangled melt dynamics. The value of ε decreases as M_w increases, with values that are vaguely indicative of actual reptation $\varepsilon < 1/2$ only being observed above $Z \simeq 10$. Thus, the onset of actual reptation is much protracted, as already deduced from NMR and dielectric data by Rössler.[28,61] In particular, a similar, smooth regime crossover characterized by a continuous mass-dependent variation of a well-defined power law exponent ranging between the pure Rouse prediction below M_e and reptation-like behavior above about 20 M_e has been observed in "pure-normal-mode" dielectric spectra of PI after suitable subtraction of the α relaxation contribution.[61]

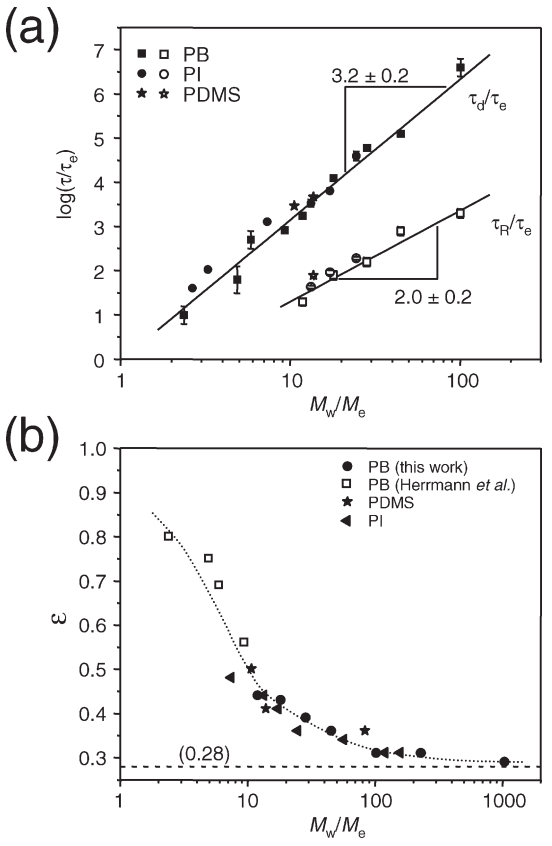

Figure 8. Universal M_w/M_e dependence of (a) the regime transition times extracted from the correlation functions and (b) the exponent in the constrained-Rouse regime, for all investigated PB, PI, and PDMS samples. The solid lines in (a) are fits in log−log units, with the given error representing the fitting uncertainty. In (b), the dotted line just guides the eye, and the dashed line indicates the apparent high-M_w plateau, which is still larger than the 1/4 predicted by the tube model.

Similar conclusions on the protracted onset of reptation can be drawn from recent computer simulations.[13,15,62] As to the origin, simulations hint at a time-dependent apparent tube diameter that increases in the regime beyond τ_e.[14] Another interpretation of probably the same phenomenon, which manifests itself as a pronounced M_w dependence of the plateau modulus at τ_e and, correspondingly, in deviations from tube-model predictions, is that the importance of CLF has so far been overestimated.[10,16] This holds in particular for short times, requiring the partial neglect of CLF[13] or an adjustment of CLF and CR time scales.[17] We note again that in our previous letter[39] dilution experiments of protonated probe chains in deuterated (invisible) matrix chains of different M_w demonstrated that the M_w dependence of ε is indeed mostly determined by the matrix, stressing the importance of CR effects even at short times, i.e., in regime II. This conclusion has recently been backed by computer simulations of similar bidisperse blends.[18]

Still, even at very high M_w, our NMR results suggest deviations from the picture of a static tube constraint in regime II. The apparent asymptotic value of $\varepsilon \sim 0.28$, being significantly larger than 0.25, is quite similar to the lowest scaling exponent $9/32 \approx 0.281$ of the mean-square displacement for $t < \tau_R$ obtained from polymer mode-coupling theory by Schweizer et al.[63] However, it remains to be shown whether the return-to-origin arguments used to convert the tube-model prediction $\langle \Delta r^2 \rangle \sim t^{1/4}$ into the

dx.doi.org/10.1021/ma1025708 |Macromolecules 2011, 44, 1549–1559

intuitive inverse $C(t) \sim t^{-1/4}$ law are also applicable in this case. In any way, the apparent deviation between a reliable experimental value and a seemingly well-accepted prediction could be taken as a serious shortcoming of tube models in general and may serve as a touchstone for future refinements.

IV. CONCLUSIONS

We have presented a consistent NMR analysis of entangled melt dynamics over 10 effective decades in time, using simple low-field equipment and a method based on dipole−dipole couplings among abundant protons, which provides a completely field-independent measure. We hope that our data may serve as a showcase of proton multiple-quantum NMR being one of the most powerful and readily available techniques to date for the quantitative study the dynamics of highly entangled polymers. We have confirmed and extended our previously published work[39] by an in-depth comparison between three different linear polymers, namely poly(butadiene), poly(isoprene), and poly(dimethylsiloxane), evaluating the applicability and shortcomings of the tube model.

In more detail, using time−temperature superposition, the method was applied to the study of chain motions over many orders of magnitude in time in terms of a segmental orientation autocorrelation function. This function is at the root of describing the dynamics in any mobile polymer system. We have here tested a well-defined prediction based on the traditional tube model and have demonstrated that the extracted regime transition times follow the expected molar mass scaling; however, the behavior in the constrained-Rouse regime II deviates in that the "tube" does not appear to be a fixed constraint at such rather short times. Rather, it is dynamic, with previous experiments on selectively isotope-labeled bidisperse blends indicating that this is a constraint-release effect, being governed by the matrix rather than the test chain itself. In addition, the method provides the amount of isotropically mobile segments, commonly associated with chain ends and connected to contour-length-fluctuation effects, which we have investigated as a function of temperature and molecular weight. The latter data suggest a mass-scaling exponent of around −0.65, which is larger than Doi's prediction of −0.5[50] but closer to previous NMR observations.[52]

Finally, we hope that our work may inspire more theoretical work on the predicion of our observed orientation autocorrelation function, which after all represents an attractive alternative to monitor describe dynamics, supplementing the more common predictions of dynamic structure factors. When this function is known, first, almost any NMR observable can be calculated, as will be further highlighted in our subsequent paper[42] concerned with an analytical prediction of the full time dependence of NMR signal functions beyond the initial-rise regime. It should be kept in mind that for networks, where the correlation function attains a well-defined plateau value at long times, its square-root is directly proportional to the cross-link density and thus the modulus. The orientation correlation function is thus of direct rheological relevance, reflecting conformational entropy, unlike the segmental mean-square displacement, the interpretation of which requires more sophisticated models. Second, in combination with recent advances in the computer simulation of the rheology of long-chain melts,[13,15,18] and hopefully also analytical theory, a comparison with a reliable NMR measure holds large potential to advance our understanding of dynamics of polymer melts and possibly other topologies such as rings, stars, or grafted architectures. A particular focus will be the further exploration of the relevance of CLF and CR effects.

AUTHOR INFORMATION

Corresponding Author

*E-mail: kay.saalwaechter@physik.uni-halle.de.

Present Addresses

†Centro de Física da Matéria Condensada Universidade de Lisboa, Lisbon, Portugal.

ACKNOWLEDGMENT

Funding of this work was provided by the Deutsche Forschungsgemeinschaft (SA 982/3-1). We are indebted to R. Graf for introducing us to the topic, many hints, and his ongoing advice and thank E. A. Rössler and A. Herrmann for valuable discussions and providing their raw data for Figure 7b. Many theory colleagues have helped us in advancing our understanding of the underlying concepts, and we explicitly thank E. Straube, S. Stepanow, and W. Paul. Infrastructure support from the European Union (ERDF programme) is gratefully acknowledged.

REFERENCES

(1) Doi, M.; Edwards, S. F. *The Theory of Polymer Dynamics*; Clarendon Press: Oxford, 1986.

(2) de Gennes, P. G. Reptation of a Polymer Chain in the Presence of Fixed Obstacles. *J. Chem. Phys.* **1971**, *55*, 572–579.

(3) Rouse, P. E., Jr. A Theory of the Linear Viscoelastic Properties of Dilute Solutions of Coiling Polymers. *J. Chem. Phys.* **1953**, *21*, 1272–1280.

(4) Kariyo, S.; Gainaru, C.; Schick, H.; Brodin, A.; Novikov, V. N.; Rössler, E. A. From a Simple Liquid to a Polymer Melt: NMR Relaxometry Study of Polybutadiene. *Phys. Rev. Lett.* **2006**, *97*, 207803.

(5) Ball, R. C.; Callaghan, P. T.; Samulski., E. T. A simplified approach to the interpretation of nuclear spin correlations in entangled polymeric liquids. *J. Chem. Phys.* **1997**, *106*, 7352–7361.

(6) Kimmich, R.; Fatkullin, N. Polymer chain dynamics and NMR. *Adv. Polym. Sci.* **2004**, *170*, 1–113.

(7) Milner, S. T.; McLeish., T. C. B. Reptation and Contour-Length Fluctuations in Melts of Linear Polymers. *Phys. Rev. Lett.* **1998**, *81*, 725–728.

(8) Likhtman, A. E.; McLeish, T. C. B. Quantitative Theory for Linear Dynamics of Linear Entangled Polymers. *Macromolecules* **2002**, *35*, 6332–6343.

(9) McLeish, T. C. B. Tube theory of entangled polymer dynamics. *Adv. Phys.* **2002**, *51*, 1379–1527.

(10) Liu, C.-Y.; Keunings, R.; Bailly., C. Do Deviations from Reptation Scaling of Entanglement Polymer Melts Result from Single- or Mainy-Chain Effects? *Phys Rev. Lett.* **2006**, *97*, 246001.

(11) Read, D. J.; Jagannathan, K.; Likhtman, A. E. Entangled Polymers: Contraint Release, Mean Paths, and Tube Bending Energy. *Macromolecules* **2008**, *41*, 6843–6853.

(12) Everaers, R.; Sukumaran, S. K.; Grest, G. S.; Svaneborg, C.; Sivasubramanian, A.; Kremer, K. Rheology and Microscopic Topology of Entangled Polymeric Liquids. *Science* **2004**, *303*, 823–826.

(13) Hou, J.-X.; Svaneborg, C.; Everaers, R.; Grest., G. S. Stress Relaxation in Entangled Polymer Melts. *Phys. Rev. Lett.* **2010**, *105*, 068301.

(14) Zhou, Q.; Larson, R. G. Direct Calculation of the Tube Potential Confining Entangled Polymers. *Macromolecules* **2006**, *39*, 6737–6743.

(15) Stephanou, P. S.; Baig, C.; Tsolou, G.; Mavrantzas, V. G.; Kröger, M. Quantifying chain reptation in entangled polymer melts: Topological and dynamical mapping of atomistic simulation results onto the tube model. *J. Chem. Phys.* **2010**, *132*, 124904.

(16) Liu, C.-Y.; He, J.; Keunings, R.; Bailly., C. Do Tube Models Yield Consistent Predictions for the Relaxation Time and Apparent

Plateau Modulus of Entangled Linear Polymers? *Macromolecules* **2006**, *39*, 3093–3097

(17) van Ruymbeke, E.; Vlassopoulos, D.; Kapnistos, M.; Liu, C.-Y.; Bailly, C. Proposal to Solve the Time−Stress Discrepancy of Tube Models. *Macromolecules* **2010**, *43*, 525–531.

(18) Baig, C.; Stephanou, P. S.; Tsolou, G.; Mavrantzas, V. G.; Kröger, M. Understanding Dynamics in Binary Mixtures of Entangled *cis*-1,4-Polybutadiene Melts at the Level of Primitive Path Segments by Mapping Atomistic Simulation Data onto the Tube Model. *Macromolecules* **2010**, *43*, 8239–8250.

(19) Perkins, T. T.; Smith, D. E.; Chu, S. Direct Observation of Tube-Like Motion of a Single Polymer-Chain. *Science* **1994**, *264*, 819–822.

(20) Adachi, K.; Wada, T.; Kawamoto, T.; Kotaka, T. Dielectric Spectroscopy on Dilute Blends of Polyisoprene/Polybutadiene: Effects of Matrix Polybutadiene on the Dynamics of Probe Polyisoprene. *Macromolecules* **1995**, *28*, 3588–3596.

(21) Zamponi, M.; Wischnewski, A.; Monkenbusch, M.; Willner, L.; Richter, D.; Likhtman, A. E.; Kali, G.; Farago, B. Molecular Observation of Constraint Release in Polymer Melts. *Phys. Rev. Lett.* **2006**, *96*, 238302.

(22) Pearson, D. S.; Fetters, L. J.; Graessley, W. W.; Ver Strate, G.; von Meerwall, E. Viscosity and Self-Diffusion Coefficient of Hydrogenated Polybutadiene. *Macromolecules* **1994**, *27*, 711–719.

(23) Pahl, S.; Fleischer, G.; Fujara, F.; Geil, B. Anomalous Segment Diffusion in Polydimethylsiloxane Melts. *Macromolecules* **1997**, *30*, 1414–1418.

(24) Komlosh, M. E.; Callaghan, P. T. Segmental motion of entangled random coil polymers studied by pulsed gradient spin echo nuclear magnetic resonance. *J. Chem. Phys.* **1998**, *109*, 10053–10067.

(25) Fischer, E.; Kimmich, R.; Fatkullin, N.; Yatsenko, G. Segment diffusion and flip-flop spin diffusion in entangled polyethyleneoxide melts: A field-gradient NMR diffusometry study. *Phys. Rev. E* **2000**, *62*, 775–782.

(26) Graf, R.; Heuer, A.; Spiess., H. W. Chain-Order Effects in Polymer Melts Probed by ^{1}H Double-Quantum NMR Spectrocopy. *Phys. Rev. Lett.* **1998**, *80*, 5738–5741.

(27) Kehr, M.; Fatkullin, N.; Kimmich, R. Deuteron and proton spin-lattice relaxation dispersion of polymer melts: Intrasegment, intrachain, and interchain contributions. *J. Chem. Phys.* **2007**, *127*, 084911.

(28) Herrmann, A.; Novikov, V. N.; Rössler, E. A. Dipolar and Bond Vector Correlation Function of Linear Polymers Revealed by Field Cycling ^{1}H NMR: Crossover from Rouse to Entanglement Regime. *Macromolecules* **2009**, *42*, 2063–2068.

(29) Brereton., M. G. NMR Transverse Relaxation Function Calculated for the Rouse Model. *Macromolecules* **1989**, *22*, 3667–3674.

(30) Brereton., M. G.; Transverse, N. M. R. Relaxation Function Calculated for Constrained Polymer Chains: Application to Entanglements and Networks. *Macromolecules* **1990**, *23*, 1119–1131.

(31) Brereton, M. G.; Ward, I. M.; Boden, N.; Wright, P. Nature of Proton NMR Transverse Relaxation Function of Polyethylene Melts. 1. Monodispersed Polyethylenes. *Macromolecules* **1991**, *24*, 2068–2074.

(32) Klein, P. G.; Adams, C. H.; Brereton, M. G.; Ries, M. E.; Nicholson, T. M.; Hutchings, L. R.; Richards., R. W. Rouse and Reptation Dynamics of Linear Polybutadiene Chains Studies by ^{2}H NMR Transverse Relaxation. *Macromolecules* **1998**, *31*, 8871–8877.

(33) Chernov, V. M.; Krasnopol'skii, G. S. Nuclear Magnetic Relaxation, Correlation Time Spectrum, and Molecular Dynamics in a Linear Polymer. *J. Exp. Theor. Phys.* **2008**, *107*, 354–366.

(34) Cohen-Addad, J. P.; Vogin, R. Molecular Motion Anisotropy as Reflected by a "Pseudosolid" Nuclear Spin Echo: Observation of Chain Constraints in Molten *cis*-1,4,-Polybutadiene. *Phys. Rev. Lett.* **1974**, *33*, 940–943.

(35) Collignon, J.; Sillescu, H.; Spiess, H. W. Pseudo-solid echoes of proton and deuteron NMR in polyethylene melts. *Colloid Polym. Sci.* **1981**, *259*, 220–226.

(36) Kimmich, R.; Fischer, E.; Callaghan, P.; Fatkullin., N. The Dipolar-Correlation Effect on the Stimulated Echo. Application to Polymer Melts. *J. Magn. Reson.* **1995**, *117*, 53–61.

(37) Callaghan, P. T.; Samulski., E. T. The Molecular Weight Dependence of Nuclear Spin Correlations in Entangled Polymeric Liquids. *Macromolecules* **1998**, *31*, 3693–3705.

(38) Cohen-Addad., J. P. NMR and Fractal Properties of Polymeric Liquids and Gels. *Prog. NMR Spectrosc.* **1993**, *25*, 1–316.

(39) Vaca Chávez, F.; Saalwächter., K. NMR Observation of Entangled Polymer Dynamics: Tube Model Predictions and Constraint Release. *Phys. Rev. Lett.* **2010**, *104*, 198305.

(40) Dollase, T.; Graf, R.; Heuer, A.; Spiess, H. W. Local Order and Chain Dynamics in Molten Polymer-Blocks Revealed by Proton Double-Quantum NMR. *Macromolecules* **2001**, *34*, 298–309.

(41) Saalwächter, K. Proton Multiple-Quantum NMR for the Study of Chain Dynamics and Structural Constraints in Polymeric Soft Materials. *Prog. NMR Spectrosc.* **2007**, *51*, 1–35.

(42) Vaca Chávez, F.; Saalwächter, K. Time-domain NMR observation of entangled polymer dynamics: Analytical theory of signal functions. *Macromolecules* **2011**, DOI:10.1021/ma102571u.

(43) Mark, J. E., Ed. *Physical Properties of Polymers Handbook*; Springer: New York, 2007.

(44) Baum, J.; Pines, A. Multiple-Quantum NMR Studies of Clustering in Solids. *J. Am. Chem. Soc.* **1986**, *108*, 7447–7454.

(45) Callaghan, P. T.; Samulski, E. T. Molecular Ordering and the Direct Measurement of Weak Proton−Proton Dipolar Interactions in a Rubber Network. *Macromolecules* **1997**, *30*, 113–122.

(46) Saalwächter, K.; Heuer., A. Chain Dynamics in Elastomers as Investigated by Proton Multiple-Quantum NMR. *Macromolecules* **2006**, *39*, 3291–3303.

(47) Anderson, P. W.; Weiss, P. R. Exchange Narrowing in Paramagnetic Resonance. *Rev. Mod. Phys.* **1953**, *25*, 269–276.

(48) Kimmich, R. *NMR Tomography, Diffusometry, Relaxometry*; Springer: Berlin, 1997.

(49) Saalwächter, K. ^{1}H multiple-quantum nuclear magnetic resonance investigations of molecular order in polymer networks: II. Intensity decay and restricted slow dynamics. *J. Chem. Phys.* **2004**, *120*, 454–664.

(50) Doi, M. Explanation for the 3.4-Power Law for Viscosity of Polymeric Liquids on the Basis of the Tube Model. *J. Polym. Sci., Polym. Phys. Ed.* **1983**, *21*, 667–684.

(51) Kornfield, J. A.; Chung, G.-C.; Smith, S. D. Reconsideration of Deuterium NMR Observations of Orientational Coupling in Polymer Networks in Light of Motional Hetergeneity in Styrene-d_8-Styrene Block Copolymers. *Macromolecules* **1992**, *25*, 4442–4444.

(52) Kimmich, R.; Köpf, M.; Callaghan, P. Components of Transverse NMR Relaxation in Polymer Melts: Influence of Chain-End Dynamics. *J. Polym. Sci., Part B: Polym. Phys.* **1991**, *29*, 1025–1030.

(53) Schillé, E.; Cohen-Addad, J.-P.; Guillermo, A. Concentrated Solutions of Partly Deuterated Triblock Polybutadiene. Segmental Analysis of NMR Properties. *Macromolecules* **2004**, *37*, 2144–2150.

(54) Saalwächter, K.; Herrero, B.; López-Manchado, M. A. Chain order and crosslink density of elastomers as investigated by proton multiple-quantum NMR. *Macromolecules* **2005**, *38*, 9650–9660.

(55) Klopffer, M.-H.; Bokobza, L.; Monnerie, L. Effect of vinyl content on the viscoelastic properties of polybutadienes and polyisoprenes − monomeric friction coefficient. *Polymer* **1998**, *39*, 3445–3449.

(56) Ferry, J. D. *Viscoelastic Properties of Polymers*; John Wiley: New York, 1980.

(57) Rubinstein, M.; Colby, R. H. *Polymer Physics*; Oxford University Press: New York, 2003.

(58) Smith, G. D.; Paul, W.; Monkenbusch, M.; Willner, L.; Richter, D.; Qiu, X. H.; Ediger, M. D. Molecular Dynamics of a 1,4-Polybutadiene Melt. Comparison of Experiment and Simulation. *Macromolecules* **1999**, *32*, 8857–8865.

(59) Hintermeyer, J.; Herrmann, A.; Kahlau, R.; Goiceanu, C.; Rössler, E. A. Molecular Weight Dependence of Glassy Dynamics in Linear Polymers Revisited. *Macromolecules* **2008**, *41*, 9335–9344.

(60) Abdel-Goad, M.; Pyckhout-Hintzen, W.; Kahle, S.; Allgaier, J.; Richter, D.; Fetters, L. J. Rheological Properties of 1,4-Polyisoprene over a Large Molecular Weight Range. *Macromolecules* **2004**, *37*, 8135–8144.

(61) Abou Elfadl, A.; Kahlau, R.; Herrmann, A.; Novikov, V. N.; Rössler., E. A. From Rouse to Fully Established Entanglement Dynamics: A Study of Polyisoprene by Dielectric Spectroscopy. *Macromolecules* **2010**, *43*, 3340–3351.

(62) Kreer, T.; Baschnagel, J.; Müller, M.; Binder., K. Monte Carlo Simulations of Long Chain Polymer Melts: Crossover from Rouse to Reptation Dynamics. *Macromolecules* **2001**, *34*, 1105–1117.

(63) Schweizer, K. S.; Fuchs, M.; Szamel, G.; Guenza, M.; Tang, H. Polymer-mode-coupling theory of the slow dynamics of entangled macromolecular fluids. *Macromol. Theory Simul.* **1997**, *6*, 1037–1117.

(64) We point out an inconsistency in our previous ref 39, where we used $\kappa = 1$ in the given equation and consequently discussed a factor of 13 as relative shift, yet the data analysis was performed with $\kappa = \pi$.